Hindawi
Shock and Vibration
Volume 2023, Article ID 2393030, 9 pages
https://doi.org/10.1155/2023/2393030

Research Article

Analysis of the Tunneling Blast Safety Criterion Based on Longitudinal Shocks

Xiao Wang, Wen-bo Zhao, Hou-you Zhou, and Dian-shu Liu

Department of Civil Engineering, China University of Mining & Technology, Beijing 100083, China

Correspondence should be addressed to Wen-bo Zhao; zwb13552337672@163.com

Received 19 February 2023; Revised 18 May 2023; Accepted 26 May 2023; Published 12 June 2023

Academic Editor: Gerardo Silva-Navarro

Copyright © 2023 Xiao Wang et al. This is an open access article distributed under the Creative Commons Attribution License, which permits unrestricted use, distribution, and reproduction in any medium, provided the original work is properly cited.

In modern tunneling construction, the blasting seismic effect seriously threatens the safety and stability of the existing engineering construction. Meanwhile, due to the complexity of blasting loading, there is a very large difference from real blasting by using the sample triangle dynamic loading model or trapezoid dynamic loading model to analyze the blasting vibration problem. In this paper, based on the analysis of the pressure change, volume expansion, fracture development, and blasting gas motion, an accurate blasting loading model was proposed. Then, adopting plane longitudinal shock theory, the coupled loading of multiple holes can be obtained. Subsequently, the 3D simulation analysis of the tunnel blasting shows an error of 2% compared with on-site monitoring data, meeting engineering requirements. Finally, based on the simulation results, regression prediction function of the velocity curve and effective tensile stress curve under different safety criteria are established, achieving accurate prediction of the damage degree of the host rock and liner line under different engineering requirements.

1. Introduction

With the swift advancement of blasting technology, as well as its excellent adaptability and affordability in various geological conditions, tunnel engineering construction by blasting accounts for over 95% of mountain tunnel construction [1]. The drilling and blasting method has become the most commonly used construction method in tunnel engineering construction. However, although the blasting method has brought significant changes to tunnel engineering construction, vibration disasters are also a major concern, especially due to the seismic effect of blasting, which is the foremost disaster [2–6]. Therefore, predicting the propagation law of blasting vibration waves has become a crucial aspect of blasting problems research [7]. At present, although scholars have made several efforts in studying the blasting propagation law, most of the studies are based on on-site monitoring data and simplified empirical formulas, which are too idealistic and lack accuracy in reflecting the actual engineering blasting vibration situation [8–10]. At the same time, some scholars also use new research methods to study the blasting vibration law, such as using neural network technology [11–13], signal noise reduction [14, 15], transient finite element analysis [16], coupled Lagrange and Euler [17], Jones–Wilkins–Lee (JWL) equation of state [18], and wavelet packet decomposition [19] to summarize the blasting vibration law. However, these methods ignore the influence of vibration frequency and duration, resulting in certain limitations. Therefore, owing to its high accuracy and affordability, numerical simulation technology has increasingly developed into an important means for engineering analysis and prediction. Many scholars worldwide have employed different numerical simulation software to simulate and analyze blasting [20–27]. Nonetheless, most of these simulations are too simplistic to reflect the actual situation of piecewise differential blasting and do not well analyze the interaction of loads between blasting holes.

This paper presents the establishment of a mathematical calculation and analysis model by analyzing the change in blasting gas pressure, the expansion of blasting hole volume, the development of surrounding rock fissures, and the movement of blasting gas in a single blasting hole, as well as the accurate form of blasting dynamic load change over time. Using the exact blast load form of a single hole, the plane

longitudinal shock wave interaction model is employed to determine the blasting load relationship under the interaction of porous holes. Finally, the finite element numerical simulation software FLAC3D is utilized to construct a 3D tunnel model, and the blasting safety criterion is obtained through the effective stress curve formula.

2. Expression of the Blasting Load Velocity

Rock is considered an incompressible medium, and it is assumed that no additional energy loss occurs during blasting. Therefore, the blasting vibration wave of a single hole in the medium propagates outward in the form of longitudinal wave concentric circles, as depicted in Figure 1.

According to the dynamic gradient theory, the propagation velocity in surrounding rock is shown in equation (28).

$$V = \sqrt{\frac{\rho_0 Q}{8\rho_r V_s}}, \frac{\overline{L}}{\sqrt{(\overline{r})^2 + (\overline{L}/2)}}, \tag{1}$$

where $V_s = \ln(\overline{L} + \sqrt{1+\overline{L}^2}/-\overline{L} + \sqrt{1+\overline{L}^2})$, $\overline{L} = (L_0/2r_0)$, $\overline{r} = (r/2r_0)$, V is the circular propagation velocity of blasting, ρ_0 is the density of the explosive, Q is the energy of blasting, ρ_r is the density of the rock, L_0 is the charge length of the blasting hole, r_0 is the radius of the blasting hole, and r is the distance from the blasting center.

3. Accurate Load Model for Blasting Analysis

The load exerted on the wall of the blasting hole after blasting is an intricate process. Following the principle of explosive initiation and action, the entire blasting process can be roughly classified into four stages: rapid increase of blasting pressure, expansion of blasting hole volume, rapid ejection of gas along the hole mouth, and completion of excavation of fracture.

3.1. The Rise Stage of the Blasting Load. After blasting, the blasting gas pressure continues to increase, resulting in a continuous increase in the dynamic load acting on the wall of the blasting hole. This study shows that when the blasting wave reaches the bottom cross section of the blasting hole, the blasting load attains the maximum, and the maximum load can be analyzed by the Chapman–Jouerger model [29].

$$P_D = \frac{1}{\gamma+1}\rho_0 V_D, \tag{2}$$

where P_D is the bursting pressure, V_D is the velocity of the explosion gas, γ is the specific heat capacity ratio of the explosion gas, and $\gamma = 3.0$ in this paper.

For the uncoupled charge, the initial burst pressure can be expressed as follows:

$$P_1 = \frac{\rho_0 V_D}{2(\gamma+1)}\left(\frac{a}{b}\right)^{2\gamma}, \tag{3}$$

where a is the diameter of the explosive cartridge and b is the diameter of the blasting hole.

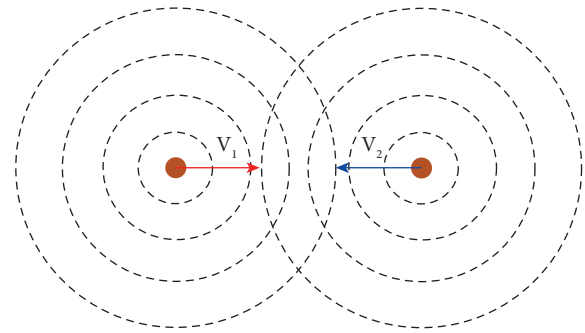

Figure 1: Plane longitudinal shock model.

The rise time of the load is as follows:

$$t_1 = \frac{L}{V_D}. \tag{4}$$

3.2. Volume Expansion of the Blast Hole. Within the blasting hole, prior to the ejection of filling material, the blasting gas causes the surrounding rock to expand, leading to the outward movement of the filling material, and an increase in the cavity volume. The volume increase can be determined by the following formula:

$$\Delta V(t) = 2\pi r(t)u(t)Ldt + 2L\int_0^{L_a}\omega(\eta)d\eta + \frac{1}{4}\pi r(t)^2 y(t), \tag{5}$$

where $r(t)$ is the radius of the blasting hole as a function of time, $u(t)$ is the expansion rate of the hole wall with time, $\omega(\eta)$ is the width of the crack, L_a is the length of the crack, and $y(t)$ is the displacement of the filling.

According to the gas fixing rate, the relationship between the gas pressure in the blasting chamber and the volume change is as follows [30]:

$$P_2 = A\left(1 - \frac{\omega}{R_1 V}\right)e^{-R_1 V} + B\left(1 - \frac{\omega}{R_2 V}\right)e^{-R_2 V} + \frac{\omega E_0}{V}. \tag{6}$$

Substituting equation (5), the rule of volume change with time, into equation (6) yields

$$\begin{aligned} P_2 = {} & A\left(1 - \frac{\omega}{R_1(V_0 + \Delta V(t))}\right)e^{-R_1(V_0+\Delta V(t))} \\ & + B\left(1 - \frac{\omega}{R_2(V_0 + \Delta V(t))}\right)e^{-R_2(V_0+\Delta V(t))} \\ & + \frac{\omega E_0}{V_0 + \Delta V(t)}, \end{aligned} \tag{7}$$

where V_0 is the initial volume of the blasting hole: A, B, R_1, R_2, and ω are the parameters of the blasting materials, and E_0 is the initial energy of the explosive.

3.3. Blasting Gas Rapid Overflow. Once the filling material in the blasting hole is ejected or in nonfilling blasting, high-pressure blasting gas will overflow rapidly along the hole

mouth. According to gas dynamics theory, the blasting hole at this stage can be simplified into the bottle-like structure as shown in Figure 2.

In the figure, $V_0, P_0, \rho_0, T_0, v_0$ are the initial volume, initial pressure, initial density, initial temperature, and initial velocity of gas in the late blasting stage, respectively, and P_e, ρ_e, T_e, v_e are the pressure, density, temperature, and velocity at the outlet, respectively. Based on gas dynamics theory, the airflow formula is as follows:

$$q_{mcr} = A\left(\frac{2}{\gamma+1}\right)^{(\gamma+1/2(\gamma+1))} + \sqrt{\gamma P_0 \rho_0}. \tag{8}$$

Assuming that the entire gas overflow process is an adiabatic process, the first law of thermodynamics is written as follows:

$$\frac{p_e(t)}{\rho_e(t)^{\gamma}} = \frac{p_e(t+dt)}{\rho_e(t+dt)^{\gamma}}. \tag{9}$$

Put the flow equation (8) into equation (9), and the following is given by the following expression:

$$p_e(t+dt) = P_e(t)\left(1 - \frac{A}{V}\left(\frac{2}{\gamma+1}\right)^{(\gamma+1/2(\gamma-1))}\frac{\sqrt{\gamma P_0 \rho_0}}{P_e(t)}dt\right). \tag{10}$$

3.4. Whole Process Analysis of the Blasting Load. At the end of blasting, the blasting energy, exerted by the blasting load, causes the surrounding rock fissure of the blasting hole to open, and the excavation of the surrounding rock mass is completed, resulting in the instantaneous scattering of the blasting gas and a rapid reduction of gas pressure to zero. Through the decomposition of the abovementioned whole blasting process and step-by-step analysis, the specific form of the blasting load action can be obtained, as shown in Figure 3.

4. Longitudinal Shock Wave Interaction Analysis

Through the abovementioned analysis, it can be seen that the blasting load in a single hole is in a nonlinear form, so the dynamic load can be approximately decomposed into the relation between amplitude P' and its second derivative P'', which is expressed in the following form [31]:

$$P = P' + P''. \tag{11}$$

The plane wave in the Lagrangian coordinate system can be expressed as follows:

$$P''_{tt} = c_0^2 P''_{\varsigma\varsigma} = G\left(P'^2\right)_{tt}, \tag{12}$$

where $c_0 = -0.1 \times 10^5 s^{-1}$ is the coefficient of wave propagation and $G = (1/\rho_0 c_0^2)[1 + (1/2)\rho_0]$. After calculation,

$$P'' = \frac{1}{2}Gt\left(P_1'^2\right)_t + \frac{1}{2}Gt\left(P_2'^2\right)_t + Gt\left(P_1' P_2'\right)_t, \tag{13}$$

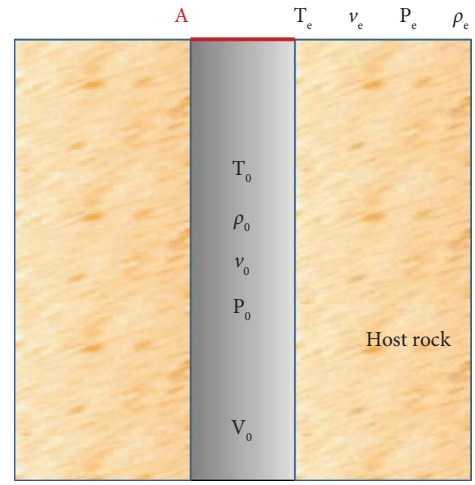

Figure 2: Model of the later blasting.

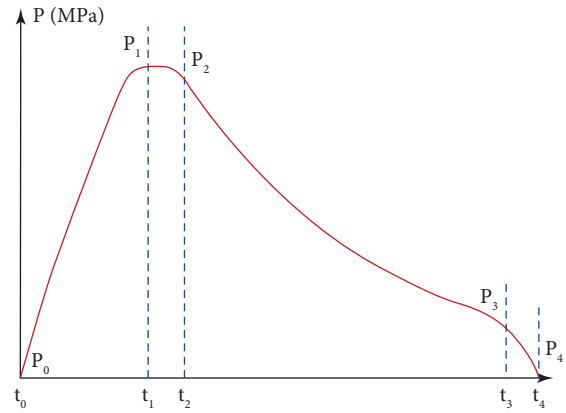

Figure 3: Model of the blasting load.

where the subscripts 1 and 2 represent the two interacting longitudinal shock waves.

A large number of experimental studies have shown that, generally, the blasting crushing zone in a rock mass is 3–5 times the radius of the blasting hole, while the blasting fracture zone is 10–15 times the radius of the blasting hole [32]. In the piecewise differential blasting of a tunnel, the direct blasting hole is usually 40 mm, and the distance between two blasting holes is approximately 60 cm, so the shock wave of the blasting hole will only be affected by the shock wave of adjacent holes. The load inside the blasting under the action of adjacent blasting holes established according to the longitudinal shock wave model is as follows:

$$P(t) = 2P'(t) + 2Gt\left(P'^2(t)\right)_t. \tag{14}$$

5. Case Study of Highway Tunnel Blasting

5.1. Engineering Background. This paper presents a case study on the blasting of a highway tunnel. The tunnel features a separate double-hole design, with the left and right lengths measuring 1075 m and 1185 m, respectively. Tunnel blasting was conducted using No. 2 rock emulsion explosive,

with a coil diameter of 32 mm, a coil length of 200 mm, and a coil weight of 150 g. The conventional blasting method was employed, with blasting holes, including cut holes, auxiliary holes, caving holes, peripheral holes, and bottom holes arranged in the tunneling end face. Among them, the cut hole is located in the middle and lower positions of the end face, and the vertical wedge cut is adopted. The spacing range of the holes was mostly 0.5–0.7 m, and the hole depth of the surrounding rock was 3.0 m. The vault of the peripheral hole utilized the interval charging method, while continuous uncoupled charging was employed at other locations, with a charging length of 2.5 m. Microdifferential section blasting was used to carry out the blasting, with the specific segmented form shown in Figure 4; the segmented time interval is shown in Table 1, and the specific blasting parameters are shown in Table 2.

5.2. Physical and Mechanical Parameters. The lithology of the surrounding rock is conglomerate, which belongs to the Houcheng Formation of the Jurassic middle system. The color is purplish red, and the structure is gravel. The gravel composition in the rock is andesite, fused tuff, rhyolite, siliceous rock, and clay rock. The gravel diameter is generally 2–60 mm, subribbed-subrounded, with good roundness and general sorting. The intergravel backfill is composed of rock debris, fine sand, and stable accessory mineral sands, such as quartz and feldspar, which are homogeneous with the gravel composition. Iron and carbonate cement between the gravel and backfill. The physical and mechanical parameters of the conglomerate are shown in Table 3.

6. Numerical Simulation Model and Data Analysis

Based on the actual engineering geological structure in the field, 3D numerical values are applied. The simulation software FLAC3D establishes the numerical model of the tunnel, as shown in Figure 5. The whole model has 372,200 units and 386,527 nodes. The model is 228 m long in the X-direction, 203 m wide in the Y-direction, and 159 m high in the Z-direction.

6.1. The Dynamic Parameters Applied in the Simulation. In the numerical simulation, based on the site monitoring data and repeated trial calculation, the measured results are compared with the trial calculation results, and the damping value that is suitable for the engineering site is obtained. The local damping coefficient of the selected calculation model in the rock and soil mass is 0.015.

6.2. Simulation Accuracy Verification. In the simulation, based on the on-site monitoring results, the simulation duration is 2 s, and a total of 1324133 steps are calculated. After calculation, the velocity curve with the same location as the on-site monitoring site is extracted and compared with the actual on-site monitoring speed curve, as shown in Figures 6 and 7.

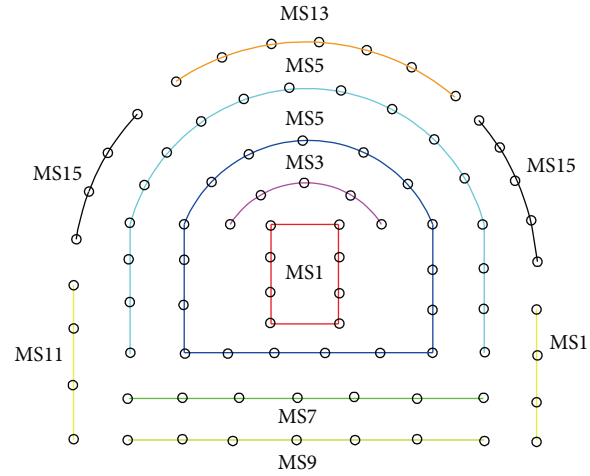

Figure 4: Position of blasting holes and segmentation.

Through the analysis of Figure 6, it can be concluded that the maximum peak intensity is 2.505 cm/s. In Figure 7, the peak intensity of field monitoring data at the same location is 2.51 cm/s, and the error rate is 2%. The arrival time of each peak of the two groups of curves was basically the same, which was between 0.3 s and 0.7 s. It can be seen from the comparative analysis that the numerical simulation based on this method is more accurate for analyzing the vibration of the surrounding rock around the blasting location and meets the analysis requirements.

6.3. Analysis of the Safety Criteria. The velocity curve and effective tensile stress curve of the rock surrounding the tunnel and along the tunnel design line are shown in Figures 8–11, respectively, and the distances from the blasting position along the tunnel design line are 10 m, 20 m, 30 m, 50 m, and 80 m, as shown in Table 4.

By summarizing the data in Table 4, the relation curves between the peak velocity and effective tensile stress in the surrounding rock and along the tunnel design line were drawn (typically at a distance of 20 m highlighted in bold in Table 4). The details are shown in Figures 12 and 13.

Figure 12 shows that the regression function of the peak velocity and effective tensile stress in the surrounding rock are as follows:

$$\sigma_t = 0.0407\,(PPV)^2 - 0.2359PPV + 0.4254, \quad R^2 = 0.9947. \tag{15}$$

According to the strength test, the dynamic tensile strength of sandstone is 4 MPa, so the surrounding rock will be damaged when the peak velocity is greater than 12.7 cm/s.

Figure 13 shows that the regression function of the peak velocity and effective tensile stress along the tunnel design line are as follows:

$$\sigma_t = 0.1188\,(PPV)^2 - 0.0406PPV + 0.1723, \quad R^2 = 0.9889. \tag{16}$$

Table 1: The time interval of every multistage.

Stage 1 (ms)	Stage 2 (ms)	Stage 3 (ms)	Stage 4 (ms)	Stage 5 (ms)	Stage 6 (ms)	Stage 7 (ms)
0	50	100	200	310	460	650

Table 2: Blasting parameters.

Cartridge diameter (mm)	Hole diameter (mm)	Number of holes	Density (kg/m^3)	Detonation velocity (m/s)	Stage
32	40	180	1000	3200	7

Table 3: Physical and mechanical parameters.

Density (kg/m^3)	Compressive strength (MPa)	Tensile strength (MPa)	Internal friction angle (°)	Poisson's ratio	Dynamic load tensile stress (MPa)
2820	75.5	3.0	75	0.2	4.0

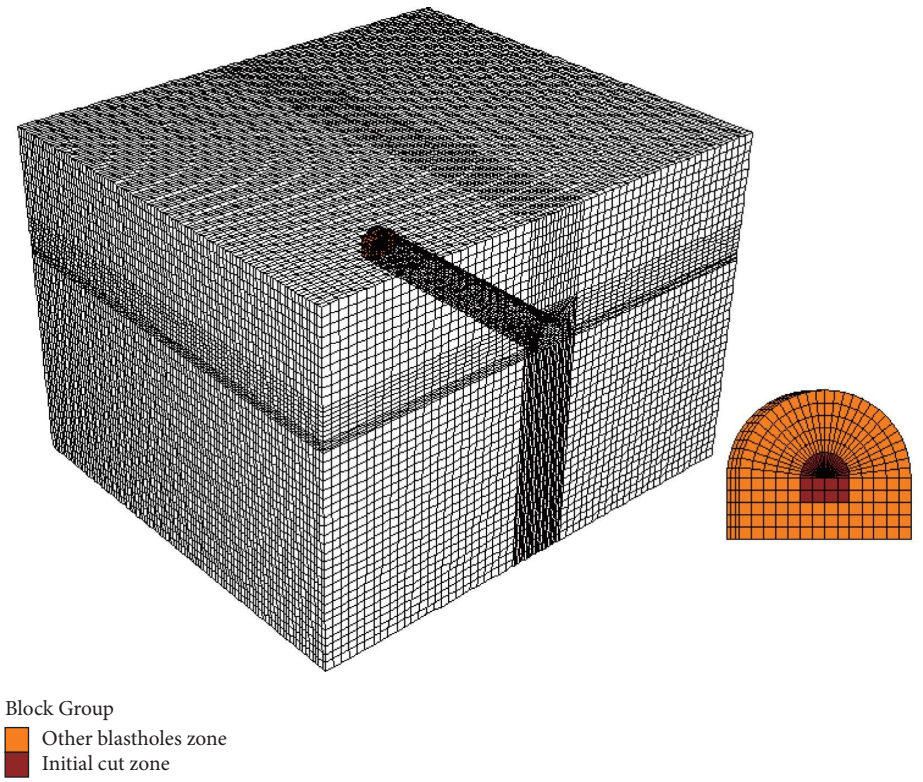

Figure 5: The 3D numerical simulation model.

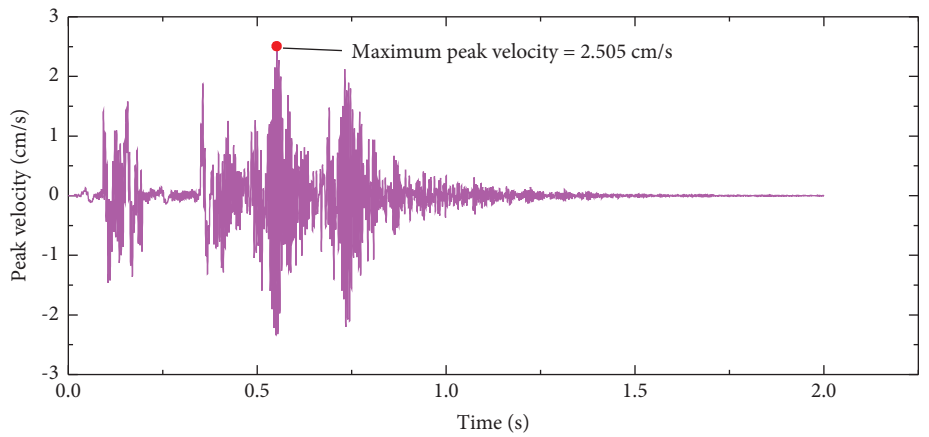

Figure 6: Simulation velocity curves of the host rock.

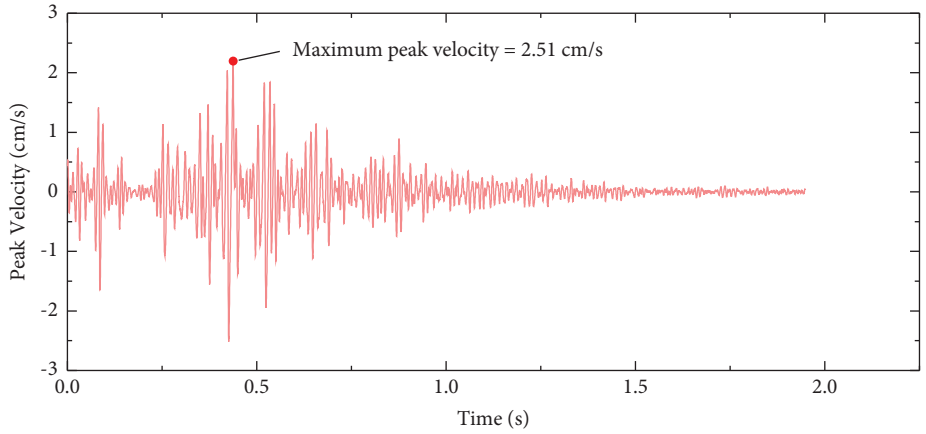

Figure 7: Monitoring velocity curves of the host rock.

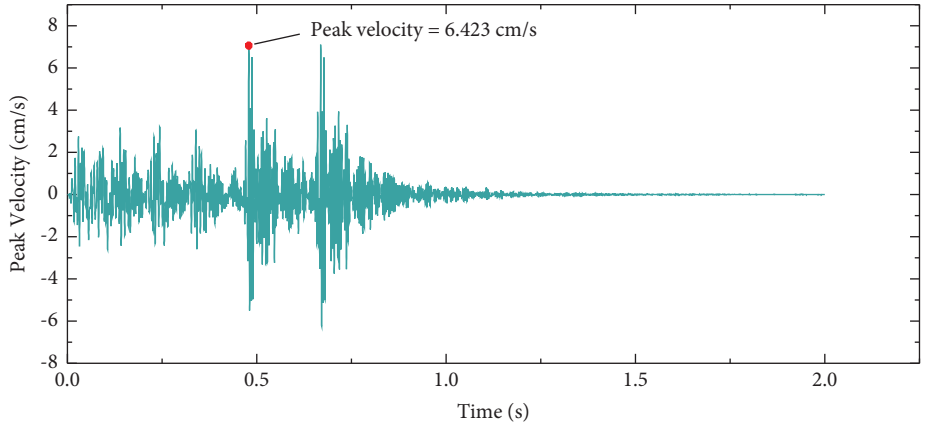

Figure 8: Velocity curve in the host rock (20 m).

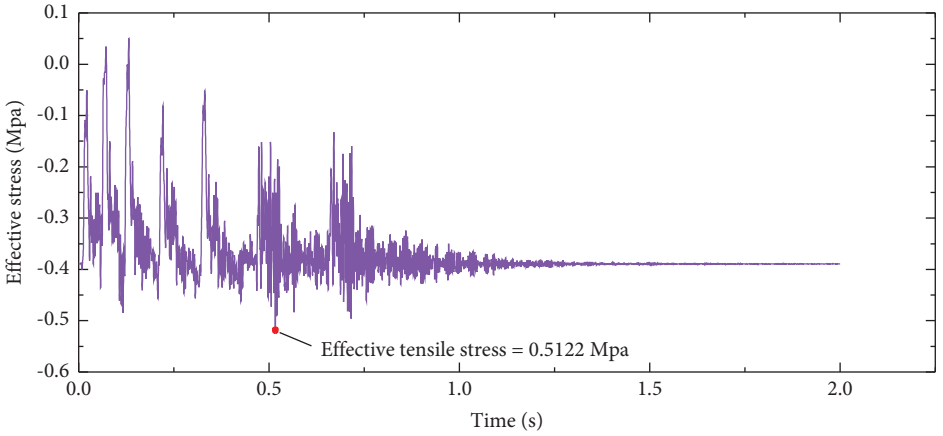

Figure 9: Effective stresses in the host rock (20 m).

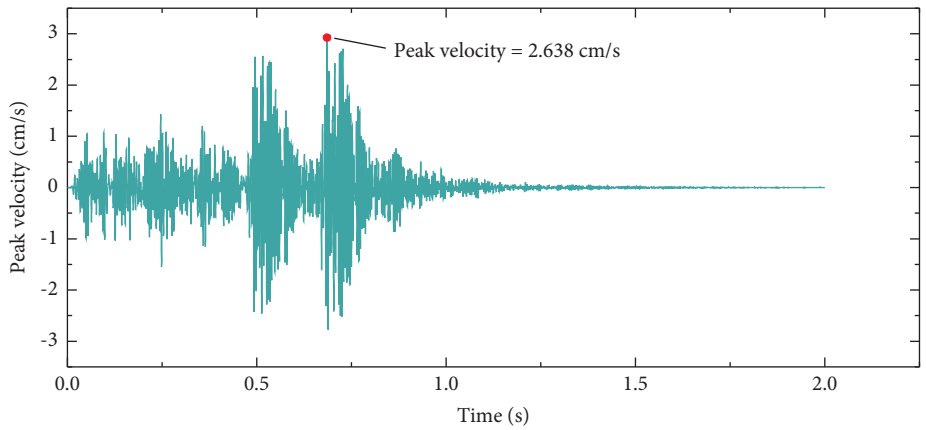

Figure 10: Velocity curves along the 20 m liner line.

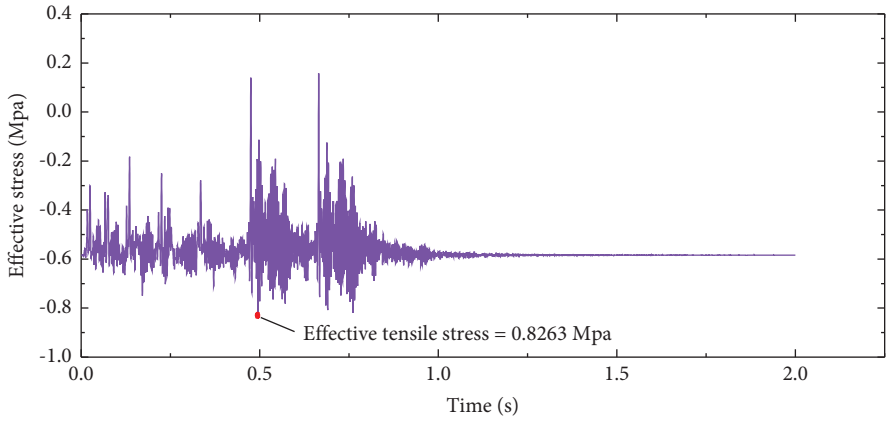

Figure 11: Effective stress curves along the 20 m liner line.

Table 4: Safety criterion data determined by the numerical simulation.

Distance (m)	Tunnel surrounding rock		Along the tunnel design line	
	Peak velocity (cm/s)	Effective tensile stress (MPa)	Peak velocity (cm/s)	Effective tensile stress (MPa)
10	10.51	2.465	3.045	1.187
20	6.423	0.5122	2.638	0.8263
30	3.218	0.1823	1.864	0.5376
50	2.505	0.1246	1.028	0.2786
80	1.321	0.1146	0.7452	0.1853

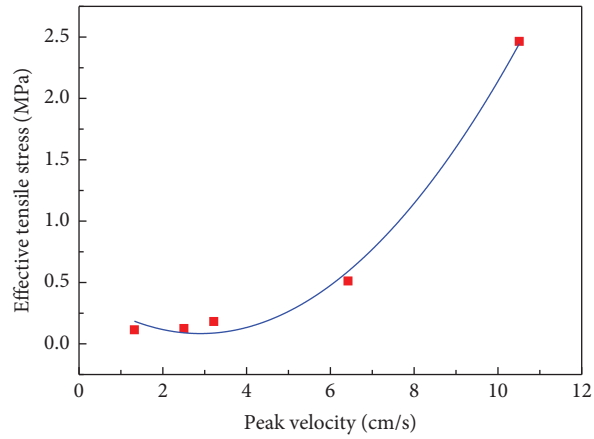

Figure 12: Safety criterion curve in the host rock.

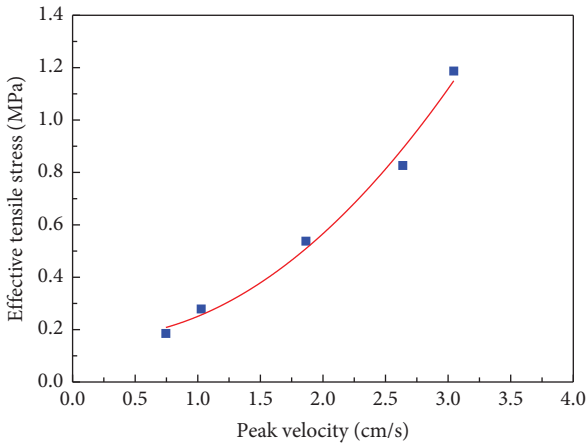

Figure 13: Safety criterion curve in the design line.

The dynamic tensile strength is 4 MPa, so the rock mass will be damaged when the peak velocity is greater than 5.85 cm/s along the tunnel design line.

7. Conclusion

This paper conducted theoretical research on the longitudinal wave shocks in tunnel blasting hole and conducts a comparison analysis between the numerical modelling result and in situ monitoring data. The following conclusion can be drawn:

(1) By establishing computational and analytical models for the changes in blasting pressure inside the blasting hole, volume expansion of the blasting hole, development of the surrounding rock fractures, and movement of blasting gas, the exact form of the time-varying blasting dynamic load was obtained. Through analysis and on-site monitoring verification, it can be seen that the variation of the dynamic load conforms more to the actual load variation than traditional triangular and trapezoidal load analysis, with significantly improved accuracy.

(2) The horizontal longitudinal shock wave interaction model was employed to analyze the porous load, and the simulation results were compared with actual monitoring data. The results show that the simulation error is within 2%, indicating that the model meets the requirements of practical analysis.

(3) By extracting the vibration velocity curve and effective tensile stress curve along the surrounding rock mass and tunnel design line, a blasting vibration safety criterion field was established, which can comprehensively reflect the damage situation of any point in the vibration field.

However, the proposed model in this paper did not take into account the complex geological information in a wide range of geological conditions and instead viewed the rock stratum as a homogeneous entity, which may not be representative of all tunneling construction scenarios. Therefore, it is necessary to consider the rock stratum conditions of the tunnel in future research and provide more practical applications to validate the effectiveness of the model.

Data Availability

The data that support the findings of this study are available from the corresponding author upon reasonable request.

Conflicts of Interest

The authors declare that they have no conflicts of interest.

Acknowledgments

This article was supported by the fund from China University of Mining and Technology, Beijing.

References

[1] S. Shen, J. Xu, S. Dai, and Y. Xu, "Extenics evaluation of joint rock tunnel blasting quality based on entropy weighting method," *Journal of Civil Engineering*, vol. 46, no. 12, pp. 118–126, 2013.

[2] R. Chaudhary, S. Mishra, T. Chakraborty, V. Matsagar, S. Mishra, and T. Chakraborty, "Vulnerability analysis of tunnel linings under blast loading," *International Journal of Protective Structures*, vol. 10, no. 1, pp. 73–94, 2019.

[3] P. Mohammadi, S. H. Khalilpour, H. Parsa, P. M. Sareh, S. H. Khalilpour, and H. Parsa, "Protective water curtains as wave attenuators for blast-resistant tunnels," *Scientific Reports*, vol. 12, no. 1, Article ID 20463, 2022.

[4] B. Wu, Y. Cui, G. Meng et al., "Research on dynamic response of shallow buried tunnel lining constructed by drilling and blasting method," *Advances in Materials Science and Engineering*, vol. 2022, Article ID 4254690, 11 pages, 2022.

[5] B. Wu, W. Qiu, W. Huang et al., "A multi-source information fusion evaluation method for the tunneling collapse disaster based on the artificial intelligence deformation prediction," *Arabian Journal for Science and Engineering*, vol. 47, no. 4, pp. 5053–5071, 2022.

[6] B. Wu, W. Qiu, W. Huang et al., "Dynamic risk evaluation method for collapse disasters of drill-and-blast tunnels: a case study," *Mathematical Biosciences and Engineering*, vol. 19, no. 1, pp. 309–330, 2022.

[7] V. Ozacar, "New methodology to prevent blasting damages for shallow tunnel," *Geomechanics & engineering*, vol. 15, no. 6, pp. 1227–1236, 2018.

[8] R. Huo, S. Li, Z. Song et al., "Analysis of vibration response law of multistory building under tunnel blasting loads," *Advances in Civil Engineering*, vol. 2019, Article ID 4203137, 16 pages, 2019.

[9] H. Luo, R. Yang, X. Ma et al., "The influence of prefabricated cracks at different angles on the propagation characteristics of main cracks in slot blasting," *Journal of Materials Engineering and Performance*, vol. 32, 2022.

[10] D. Guo, W. Xiao, D. Guo, Y. Lu, D. Guo, and Y. Lu, "Numerical simulation of surface vibration propagation in tunnel blasting," *Mathematical Problems in Engineering*, vol. 2022, Article ID 3748802, 10 pages, 2022.

[11] E. Trigueros, M. Cánovas, J. Muñoz, J. Cospedal, J. M. Munoz, and J. Cospedal, "A methodology based on geomechanical and geophysical techniques to avoid ornamental stone damage caused by blast-induced ground vibrations,"

International Journal of Rock Mechanics and Mining Sciences, vol. 93, pp. 196–200, 2017.

[12] L. He, D. Kong, Z. Z. Lei, and Z. Lei, "Research on vibration propagation law and dynamic effect of bench blasting," *Mathematics*, vol. 10, no. 16, p. 2951, 2022.

[13] Y. Fan, Y. Pei, G. Yang, Z. Leng, and W. Lu, "Prediction of blasting vibration velocity peak based on an improved PSO-BP neural network," *Journal of Vibration and Shock*, vol. 41, no. 16, pp. 194–203, 2022.

[14] C. Yu, H. Yue, H. Li et al., "Scale model test study of influence of joints on blasting vibration attenuation," *Bulletin of Engineering Geology and the Environment*, vol. 80, no. 1, pp. 533–550, 2021.

[15] Z. Wang, C. Fang, Y. Chen, W. Cheng, Y. Chen, and W. Cheng, "A comparative study of delay time identification by vibration energy analysis in millisecond blasting," *International Journal of Rock Mechanics and Mining Sciences*, vol. 60, pp. 389–400, 2013.

[16] K. Mosalam, A. S. M. Mosallam, and A. S. Mosallam, "Nonlinear transient analysis of reinforced concrete slabs subjected to blast loading and retrofitted with CFRP composites," *Composites Part B: Engineering*, vol. 32, no. 8, pp. 623–636, 2001.

[17] G. Yang, G. Wang, W. Lu, P. Yan, and M. Chen, "Damage assessment and mitigation measures of underwater tunnel subjected to blast loads," *Tunnelling and Underground Space Technology*, vol. 94, Article ID 103131, 2019.

[18] P. Keshavarz Mirza Mohammadi, S. H. Khalilpour, H. Parsa, P. H. Sareh, and H. Parsa, "Computational performance evaluation of sacrificial protective walls composed of lightweight concrete blocks: a parametric study of blast loads in a tunnel," *Mechanics of Advanced Materials and Structures*, vol. 2022, Article ID 2125134, 15 pages, 2022.

[19] T. Ling, X. Li, T. Dai et al., "Features of energy distribution for blast vibration signals based on wavelet packet decomposition," *Journal of Central South University of Technology*, vol. 12, no. 1, pp. 135–140, 2005.

[20] S. Kim, W. Jeong, D. Jeong, J. Seok, D. Jeong, and J. Seok, "Numerical simulation of blasting at tunnel contour hole in jointe rock mass," *Tunnelling and Underground Space Technology*, vol. 21, no. 3-4, pp. 306-307, 2006.

[21] Q. Ding, B. Li, H. Su et al., "Damage mechanism and stability analysis of rock mass in the high geo-stress tunnel subjected to excavation," *Geomatics, Natural Hazards and Risk*, vol. 13, no. 1, pp. 75–93, 2022.

[22] J. Zhou, X. Yang, J. Guo, and J. Guo, "Stability predictions for excavations of mountain tunnels based on [BQ] method and its field verification," *Engineering Failure Analysis*, vol. 141, Article ID 106727, 2022.

[23] M. Ziegler, A. Alimardani Lavasan, S. Loew, A. A. Lavasan, and L. Simon, "Stress evolution around a TBM tunnel in swelling clay shale over four years after excavation," *Tunnelling and Underground Space Technology*, vol. 128, Article ID 104649, 2022.

[24] P. Keshavarz Mirza Mohammadi, S. H. Khalilpour, and P. Sareh, "Simulating the response of buried structures to external blast loads: methods, challenges, and advances," *Engineering Reports*, vol. 12, Article ID e12607, 2022.

[25] M. Eslami, P. Keshavarz MirzaMohammadi, S. H. Khalilpour, H. Parsa, and V. H. Kodure, "Experimental and numerical investigation of blast wave attenuation by using barriers in different configurations and shapes," *Journal of Structural Engineering*, vol. 149, no. 1, Article ID 04022224, 2023.

[26] A. Altunışık, F. Önalan, F. Sunca, F. Önalan, and F. Sunca, "Effects of concrete strength and openings in infill walls on blasting responses of RC buildings subjected to TNT explosive," *Iranian Journal of Science and Technology, Transactions of Civil Engineering*, vol. 45, no. 4, pp. 2525–2554, 2021.

[27] K. Ma, J. Zhang, P. Zhou et al., "Floor heave failure mechanism of large-section tunnels in sandstone with shale stratum after construction: Floor heave failure mechanism of large-section tunnels in sandstone with shale stratum after construction: A case study case study," *Engineering Failure Analysis*, vol. 140, Article ID 106497, 2022.

[28] Q. Gao, C. Liu, J. Zhang, G. Cheng, J. Zhang, and G. Cheng, "Simulating the formation of blasting-excavation-induced zonal integration in deep tunnels with an elastoplastic damage model," *Shock and Vibration*, vol. 2021, pp. 9991251–18, 2021.

[29] P. Afanasev, K. F. I. Makhmudov, and K. F. Makhmudov, "Assessment of the parameters of a shock wave on the wall of an explosion cavity with the refraction of a detonation wave of emulsion explosives," *Applied Sciences*, vol. 11, no. 9, p. 3976, 2021.

[30] W. Zheng, L. Pang, Y. Liu et al., "Effects of initial condition and fuel composition on laminar burning velocities of blast furnace gas with low heat value," *Fuel*, vol. 289, Article ID 119775, 2021.

[31] Y. Mukha, A. L. P. Surkaev, and A. L. Surkaev, "Studying the effect of nonlinearity of interacting acoustic shock waves," *Technical Physics Letters*, vol. 28, no. 8, pp. 640-641, 2002.

[32] M. Shadabfar, C. Gokdemir, M. Zhou et al., "Estimation of damage induced by single-hole rock blasting: a review on analytical, numerical, and experimental solutions," *Energies*, vol. 14, no. 1, p. 29, 2020.